The Effect of Iodide and Chloride on Transthyretin Structure and Stability[†,‡]

Andreas Hörnberg, Ulrika W. Hultdin, Anders Olofsson, and A. Elisabeth Sauer-Eriksson*

From Umeå Centre for Molecular Pathogenesis, Umeå University, SE-901 87 Umeå, Sweden

Received February 10, 2005; Revised Manuscript Received May 11, 2005

ABSTRACT: Transthyretin amyloid formation occurs through a process of tetramer destabilization and partial unfolding. Small molecules, including the natural ligand thyroxine, stabilize the tetrameric form of the protein, and serve as inhibitors of amyloid formation. Crucial for TTR's ligand-binding properties are its three halogen-binding sites situated at the hormone-binding channel. In this study, we have performed a structural characterization of the binding of two halides, iodide and chloride, to TTR. Chlorides are known to shield charge repulsions at the tetrameric interface of TTR, which improve tetramer stability of the protein. Our study shows that iodides, like chlorides, provide tetramer stabilization in a concentration-dependent manner and at concentrations approximately 15-fold below that of chlorides. To elucidate binding sites of the halides, we took advantage of the anomalous scattering of iodide and used the single-wavelength anomalous dispersion (SAD) method to solve the iodide-bound TTR structure at 1.8 Å resolution. The structure of chloride-bound TTR was determined at 1.9 Å resolution using difference Fourier techniques. The refined structures showed iodides and chlorides bound at two of the three halogen-binding sites located at the hydrophobic channel. These sites therefore also function as halide-binding sites.

The human plasma protein transthyretin (TTR)[1] is predominantly expressed in the liver and the choroid plexus of the brain. TTR is a homotetrameric protein of 55 kDa and functions as a transporter protein for the thyroid hormone thyroxine (T_4) and retinol (vitamin A) in complex with the retinol binding protein (RBP) (for reviews see refs *1*−*3*). Recently, TTR has also been found to possess proteolytic activity, which might be of physiological relevance (*4*). The thyroid transport function of TTR is carried out together with two more proteins, albumin and thyroxine-binding globulin. Combined, the three proteins maintain the equilibrium between extracellular and cellular hormone pools. The T_4-binding globulin is the major T_4 carrier and binds around 75% of all T_4 present in plasma (*5*). Only about 10−25% of all TTR tetramers present in plasma carry T_4, which makes the role of TTR in T_4 transport less obvious (*6*) and suggests that it is more important as a molecule for vitamin A transport. In cerebrospinal fluid, however, TTR is the main T_4-binding protein, which suggests that it has a more vital role in the central nervous system (*7*, *8*).

In certain individuals, TTR is converted into an insoluble, but highly ordered, fibrillar structure referred to as amyloid. TTR-amyloid formation is associated with the development of several diseases (*9*, *10*). Familial amyloidotic polyneuropathy (FAP) and familial amyloidotic cardiomyopathy (FAC) are caused by single point mutations in the transthyretin gene. There are now over 70 such mutations identified (see refs *11*−*13* and references therein). One of the most clinically significant of these is the substitution of methionine for valine at position 30 (ATTR V30M). TTR also causes senile systemic amyloidosis (SSA), which is a milder condition in comparison with FAP and FAC and related to amyloid fibrils formed by the wild-type protein (*14*). This suggests that TTR mutations accelerate fibril formation and are not necessarily responsible for initiation of fibril formation. Cell toxicity is associated with early stages of TTR fibril formation, and mature full-length fibrils may therefore represent an inert end stage, which serves as a rescue mechanism for the cell (*15*, *16*).

The structure of human wild-type TTR is well-characterized (*17*−*19*) and so are many of the mutants known to cause disease (*18*, *20*−*25*). TTR is a homotetrameric protein in which each of the four monomers of 127 amino acids forms an immunoglobulin-like β-barrel structure (Figure 1A) (*17*). The retinol-binding protein binds to the α-helix at the surface of the TTR molecule (*26*−*28*), while the thyroxine-binding site is positioned in the hydrophobic channels at the TTR dimer−dimer interface (*29*−*31*). From the interaction of the four iodine substituents of T_4 with the hydrophobic channel of TTR, three halogen-binding pockets (HBP1−3) were identified in the crystal structure (*29*).

Human TTR tetramers can, in vitro, be partially separated into monomers under acidic conditions. At low pH, amyloid fibril assembly is observed, which suggests a model for

[†] This study was supported by the Swedish Science Council (K2004-03X-13001-06A, K2004-03EF-15196-01A, K2004-03B-15003-01A), Socialstyrelsen, M. Bergvalls foundation, Hjärnfonden, and the patients' association FAMY/AMYL.

[‡] Atomic coordinates and structure factors have been deposited in the Research Collaboratory for Structural Bioinformatics (RCSB) with the following accession codes 1ZCR (wtTTR-iodide complex) and 1ZD6 (wtTTR-chloride complex).

* To whom correspondence should be addressed. E-mail: liz@ucmp.umu.se. Phone: +46-90-7856782. Fax: +46-90-778007.

[1] Abbreviations: TTR, transthyretin; ATTR, TTR associated with amyloidosis in vivo, FAP, familial amyloidotic polyneuropathy; SSA, senile systemic amyloidosis; T_4, 3,5,3′,5′-tetraiodo-L-thyronine (thyroxine); T_3, 3,5,3′-triiodo-L-thyronine; RBP, retinol binding protein; TBG, thyroxine-binding globulin; rms, root-mean-square; AFM, atomic force microscopy.

10.1021/bi050249z CCC: $30.25
Published on Web 06/09/2005

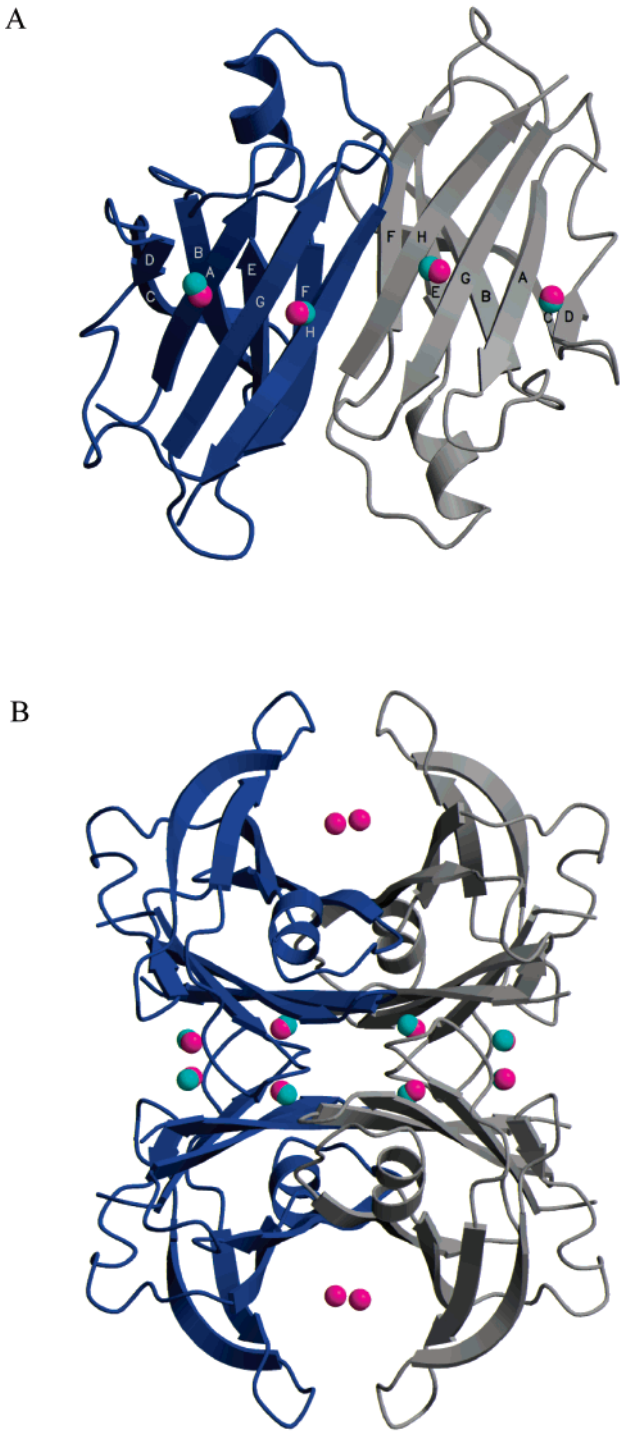

FIGURE 1: The three-dimensional structure of TTR displayed as a (A) dimer and (B) tetramer. The model is drawn from the iodide−TTR structure. Each of the four monomers comprises eight β-strands denoted A−H (labeled as in the original structure (*17*)) and one short α-helix. The β-strands are organized in two β-sheets comprising four β-strands each (D-A-G-H and C-B-E-F) in a topology similar to the classic Greek key β-barrel. The bound iodides are shown as pink spheres. Chloride atoms from the chloride−TTR structure were superimposed on the iodide−TTR structure and are shown as turquoise spheres.

amyloid formation based on misfolded monomers that build the amyloid fibril (*32*−*35*). Other studies demonstrate that transthyretin amyloid fibrils may assemble from oligomeric protein building blocks rather than restructured monomers (*36*−*41*). All models, however, support the currently most successful approach for preventing TTR amyloid formation, that is, increasing the kinetic barrier associated with misfolding, thereby preventing amyloidogenesis by stabilization of the native tetrameric conformation (*42*−*45*). Small inhibitor molecules that bind to one or both of the unoccupied T_4-binding sites of TTR have been shown to stabilize the native state and reduce the rate of amyloid formation (*44*, *46*−*48*). Binding of the natural ligand T_4 has also been shown to stabilize the tetrameric structure of TTR and inhibit amyloid formation in vitro under acidic conditions (*42*, *49*).

The precursor molecules for thyroxine synthesis are iodide ions and tyrosyl residues. So far, no studies have been reported on the effect of iodide binding on human TTR. It has, however, been shown that electrostatic repulsion between two pairs of equivalently positioned Lys15 residues destabilizes the tetrameric structure of TTR and that anions such as chlorides shield these charge repulsions and improve tetramer stability (*50*). In this paper, we show that iodide increases tetramer stabilization and reduces protein aggregation in vitro at lower concentrations compared to chloride. We also describe two crystal structures of human TTR with bound chloride and iodide, respectively. From these structures, three halide-binding sites were identified per TTR monomer, of which two are situated at the halogen-binding sites and the third at the surface of the monomer in a region referred to as the saddle (Figure 1B). The presence of halide-binding sites in human TTR provides new insight into the possible role of anions in TTR tetramer stabilization.

MATERIAL AND METHODS

Protein Purification. Recombinant human wild-type TTR (wtTTR) was expressed as previously described (*19*). Briefly, the bacteria were grown in LB medium and induced by isopropyl-β-D-thiogalactopyranoside (IPTG) for 3 h before harvesting by centrifugation. The pellet was resuspended in a small volume (10 mL/L culture) of 50 mM Tris-HCl, pH 7.5, and frozen at −80 °C. The frozen cells were thawed and resuspended in 50 mM Tris-HCl, pH 7.0, and 50 mM NaCl, which efficiently ruptured the cell membrane. After lysis, DNAse was added in the presence of Mn^{2+} ions followed by centrifugation at 20 000*g* for 20 min. The supernatant was loaded on a MonoQ anion-exchange column (Amersham Biotech), using 20 mM Tris, pH 6.8, as a running buffer. The protein was eluted with 0.3 M NaCl applying a gradient from 0 to 1.0 M NaCl. Fractions containing >80% pure protein were concentrated (Centriprep, Amicon) and loaded on a size-exclusion column (Superdex-G75, GE health care) in 5 mM phosphate buffer, pH 7.0. Pure fractions were pooled and frozen in liquid N_2.

Urea-Mediated Denaturation Curves. The stability of wtTTR was investigated at various concentrations of KI and KCl as a function of urea following a previously described protocol (*50*). Briefly, unfolding of TTR exposes two buried tryptophan residues. Native and unfolded TTR therefore exhibit tryptophan fluorescence maxima at different wavelengths, 335−337 nm and 355−358 nm, respectively, and denaturation of TTR can be followed as the 355:335 emission intensity ratio (*50*). In our experiments, the protein (0.2 mg/mL, in 50 mM sodium phosphate buffer, pH 7.0, 1 mM EDTA, and 1 mM DTT) was incubated for 96 h at 25 °C with freshly prepared urea 0−7 M in the presence of different

concentrations of KI (0−0.5 M) or KCl (0−1.5 M). Trp fluorescence spectra of TTR, after excitation at 295 nm, were recorded over the range of 310−410 nm using a Fluoromax Jobin Yvon-spex (ISA) spectrofluorometer equipped with a thermostated cell holder. The dissociation rates of wtTTR in 0.1 M KI or 0.1 M KCl were studied in 6 M urea and measured over 96 h at 25 °C.

Fibril Formation under Acidic Conditions. The amyloidogenicity of wtTTR was evaluated with and without chloride and iodide ions. Using a previously described protocol (*32*, *42*), we diluted purified human wtTTR (in 10 mM sodium phosphate, pH 7.0) to a final concentration of 0.2 mg/mL in buffers appropriate for the desired pH (e.g., 50 mM NaOAc, 1 mM EDTA, and 1 mM DTT) with the addition of various concentrations of KI or KCl. After 72 h at 37 °C, all samples were vortexed before measuring the optical density (OD) at 400 nm.

Crystallization, Data Collection, and Structure Determination of Iodide- and Chloride-Bound Transthyretin. Crystals of iodide-bound wtTTR were obtained by the hanging drop vapor-diffusion method (*51*). Four microliters of 3 mg/mL protein in 50 mM Tris-HCl, pH 7.5, was mixed with 2 μL of a well solution containing 1.4 M $(NH_4)_2SO_4$ (AS), 0.4 M NaI, 0.1 M Na Citrate, pH 5.0, and 2% poly(ethylene glycol) (PEG) 200. Crystals of $0.3 \times 0.6 \times 0.6$ mm^3 appeared after 5−10 days at 18 °C.

One cryo-cooled crystal (*52*) was used to collect a 1.8 Å data set using Cu Kα radiation generated from an in-house Nonius FR 591 fine focus rotating anode generator on a MAC Science double image plate 2030H. Over 400 degrees of data were collected to ensure high completeness and redundancy. The images were processed and scaled using the DENZO/SCALEPACK program package (*53*). Despite the amount of data, R_{merge} did not fluctuate during data processing. Details of the data collection statistics are given in Table 1. The structure was solved with the single-wavelength anomalous dispersion (SAD) method as implemented in the CNS program package (*54*). Five percent of the reflections was randomly excluded and used as a test set to monitor the refinement process as *R*-free (*55*). The heavy atom search showed six iodides in the asymmetric unit (three per monomer), and their anomalous signals were sufficient to solve the structure. Initial automated model building was performed with ARP/wARP warpNtrace (*56*, *57*) and resulted in the proper placement of 91% of the residues. Refinement was done using conjugate gradient minimization and simulated annealing, as implemented in CNS, alternated with manual rebuilding of the model using the program O (*58*). The structure was further refined with the program REFMAC, part of the CCP4 program package (*59*) using the maximum likelihood residual, anisotropic scaling, bulk-solvent correction, and atomic displacement parameter refinement (*60*) and the translation, libration, screw-rotation (TLS) method (*61*, *62*). The details of the refinement statistics are included in Table 1.

Crystals in the presence of chloride were grown in the same conditions as the above crystals except that 1.8 M AS and 0.5 M NaCl were substituted for 1.4 M AS and 0.4 M NaI, respectively. The structure from these crystals was solved by difference Fourier methods and showed low binding of chlorides in the hormone-binding channel. Crystals were therefore soaked for 2 days in well solution containing 1.5 M NaCl prior to data collection to intensify the binding. This structure was refined using a similar protocol as described for the iodide-bound TTR structure. Refinement statistics are shown in Table 1.

Table 1: Data Collection, Refinement and Structural Statistics

	iodide complex	chloride complex
	Data collection	
space group	$P2_12_12$	$P2_12_12$
unit cell (Å) *A, B, C*	43.38, 86.26, 64.44	42.66, 85.59, 63.49
number of reflections	702086	345745
unique reflections	22882	18946
resolution range (Å)	20−1.8 (1.86−1.8)	20−1.9 (1.97−1.90)
completeness (%)	99.9 (100)	100 (100)
R_{merge}[a]	5.7 (23.7)	8.6 (57.5)
$I/\sigma I$	32.7 (3.7)	27.0(3.9)
	Refinement	
reflections work set	21705	17967
reflections test set	1177	979
R factor[b]	20.3 (24.6)	20.0 (23.2)
R_{free}[c]	23.8 (26.3)	22.1 (24.4)
no. of water molecules	136	136
mean *B* factor (Å^2)		
protein dimer	12.00	16.51
water molecules	27.03	33.09
ions	31.00	32.00
occupancies (%) and {σ} values of:		
ion 1	75 {17}	67 {6}
ion 2	21 {6}	37 {3}
ion 3	50 {14}	55 {5}
ion 4	91 {22}	69 {7}
ion 5	38 {11}	41 {4}
ion 6	47 {12}	65 {6}
rms deviation for bond lengths (Å)[d]	0.006	0.007
rms deviation for bond angles (°)	1.267	1.327
Ramachandran angles		
most favored (%)	90.5	89.6
allowed (%)	9.5	10.4
	Structure	
rms deviation compared to wtTTR (pdb code 1F41)[e]	0.181	0.228
rms deviation compared to chloride	0.240	-

[a] $r_{merge} = \sum_h\sum_i|I_h - \langle I_h\rangle|\sum_h\sum_i \cdot I_h\rangle$, where $\langle I_h\rangle$ is the mean intensity of the *i* observations of reflection *h*. The values in bracket are for reflections from the highest resolution shell. [b] *R*-factor $= \sum||F_{obs}| - |F_{calc}||/\sum|F_{obs}|$, where $|F_{obs}|$ and $|F_{calc}|$ are the observed and calculated structure factor amplitudes, respectively. Summation includes all reflections used in the refinement. [c] $R_{free} = \sum||F_{obs}| - |F_{calc}||/\sum|F_{obs}|$, evaluated for a randomly chosen subset of 5% of the diffraction data not included in the refinement. [d] Root-mean-square deviation from ideal values. [e] The main-chain atoms (N, Cα, C, O) of residues A-Cys10-Asn98 and A-Arg104-Thr123 were used in the calculations.

RESULTS

Urea Denaturation. Urea unfolding of wtTTR in the absence or presence of salt was monitored by tryptophan fluorescence at pH 7.0 (Figure 2A,B). In agreement with previous results (*50*), our experiment showed that chloride stabilized TTR in a concentration-dependent manner, and at 1.5 M chloride, it was not possible to denature the protein even at 6 M urea (Figure 2A). Substituting iodide for chloride, the same stabilization effect could be obtained already at 0.1 M iodide (Figure 2B,C).

Partial Denaturation of Transthyretin. The propensity for TTR-amyloid fibril formation was measured as a function

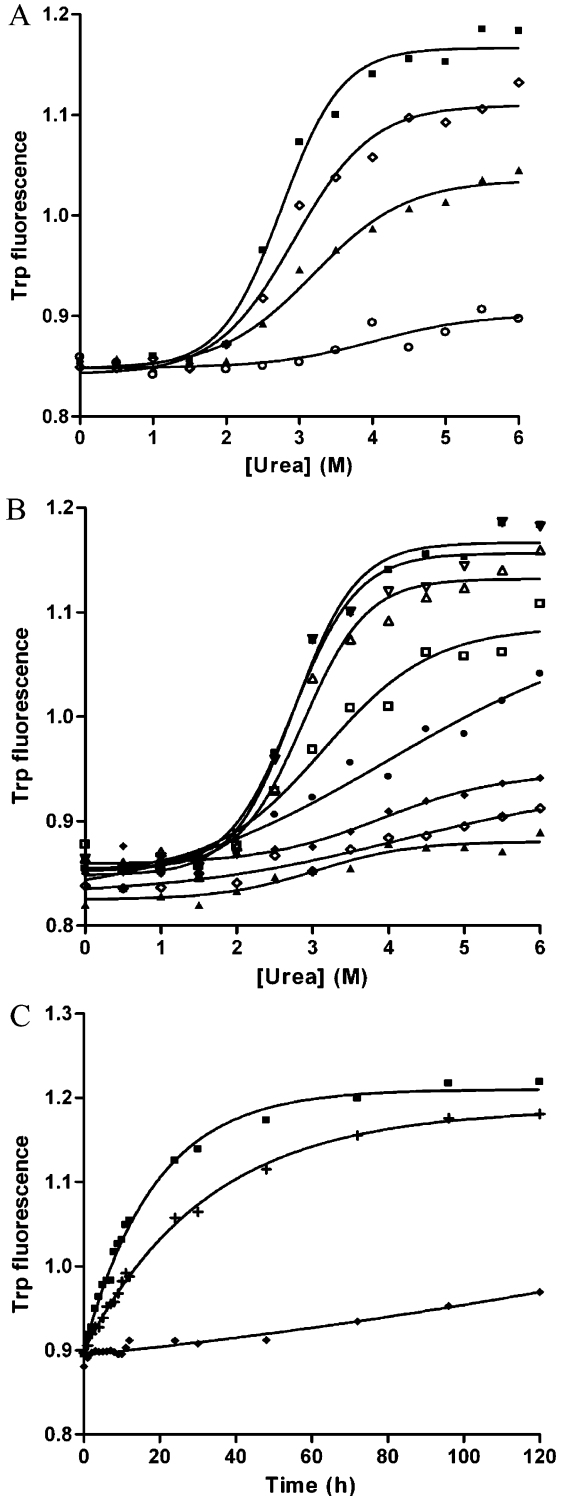

FIGURE 2: (A and B) Urea unfolding of wtTTR (0.2 mg/mL, pH 7.0) at various concentrations of KCl and KI. The degree of unfolding is displayed as the ratio of tryptophane fluorescence intensity measured at 355 and 335 nm after excitation at 295 nm (*50*). (A) Added KCl: 0.0 (■), 0.25 (◇), 0.5 (▲), and 1.5 M (○). (B) Added KI: 0.0 M (■), 1 mM (▽), 2.5 mM (△), 10 mM (□), 25 mM (●), 0.1 M (◆), 0.25 M (◇), and 0.5 M (▲). (C) TTR denaturation in 6.0 M urea in the absence and presence of salt: 0.0 M (■), 0.1 M KCl (+), and 0.1 M KI (◆). The extent of unfolding was followed by tryptophane fluorescence as described in panels A and B.

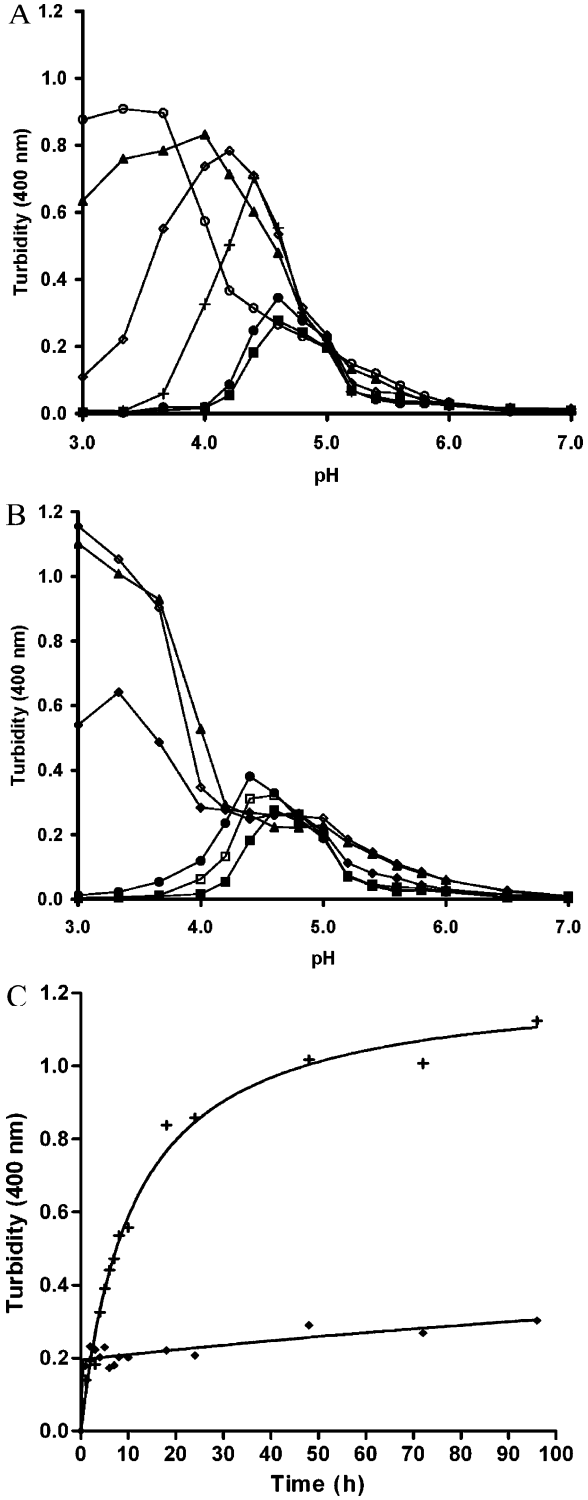

FIGURE 3: Aggregation of human TTR as a function of pH at various concentrations of salt. (A) Added KCl: 0.0 M (■), 25 mM (●), 0.1 M (+), 0.25 M (◇), 0.5 M (▲), and 1.5 M (○). (B) Added KI: 0.0 M (■), 10 mM (□), 25 mM (●), 0.1 M (◆), 0.25 M (◇), and 0.5 M (▲). The turbidity was measured at 400 nm after incubation of protein samples for 72 h. (C) Aggregation of human TTR as a function of time: 0.1 M KCl (+) and 0.1 M KI (◆).

of pH at various concentrations of KCl or KI (Figure 3A,B) by monitoring the optical density at 400 nm. Previous investigations have shown that wtTTR forms fibrils after prolonged incubation at low pH in 37 °C and that the level of fibrillization essentially correlates with the optical density of the precipitates (*63*). In the presence of 0.1 M Cl^- and at a protein concentration corresponding to 0.2 mg/mL, the maximum yield occurs at pH 4.4 (*32*). Our results, obtained after varying both pH and salt, suggested that synergistic

effects influenced the turbidity and made the interpretations more complex. At low concentrations of Cl^- ions, the turbidity curves essentially followed the previously reported Gaussian distribution associated with amyloid fibril formation (*32*). At physiological salt concentrations, the pH was 4.4 for maximum turbidity, which is in agreement with previous published result (*32*). Moreover, in the absence of salt, the turbidity for wild-type TTR was slightly shifted to reach its maximum at pH 4.6−4.8, which is close to the calculated isoelectric point (pH 4.6−4.9) of tetrameric TTR (*64*). The result is furthermore in accordance with a less stable tetramer in absence of salt due to the anion shielding of Lys15 (*50*). At 0.1−0.2 M Cl^-, the curves reached higher amplitudes suggesting that aggregation at this pH range is stimulated by the increased ion strength. At chloride concentrations higher than 0.5 M, the effect was even more pronounced and significant amounts of precipitates were observed also at pH values below 4. Plausibly, this precipitation is due to a salting-out effect in combination with a partial denaturation as a result of the low pH. Substituting iodide for chloride led to similar results; however, only a minor increase in turbidity was observed at pH range 4.0−5.0 in the presence of 0.1 M iodide. At this concentration, the direct binding of iodides to the protein leads to a more stabilized tetrameric structure (Figure 3B). Chloride, however, does not bind to the protein at the same extent at this concentration and, consequently, fibrillization increased. We note that iodide ions are less efficient salting-out agents according to the Hofmeister series. At pH below 4.0, a significant increase in turbidity could be observed already at an iodide concentration corresponding to 0.1 M (Figure 3B). In comparison with the results obtained from chloride experiments and with respect to the Hofmeister series of ion interactions, the results are inconclusive and need further elucidation. At present, we can only conclude that multiple factors appear to control the aggregation and precipitation of TTR. Using atomic force microscopy (AFM), we were not able to detect fibrils in the precipitate formed in our experiments. However, this does not exclude the possibility that fibrillar structures were embedded within the large aggregates.

It has been established that the kinetics of tetramer dissociation is the major rate-limiting step in TTR fibril formation (*35*). As a consequence, the effect of including iodide ions while monitoring the rate of fibril formation was investigated using the above-described assay where the change in turbidity was followed over time at a constant pH of 4.4. The result showed a clear difference in the aggregation-rate of wtTTR where 0.1 M iodide significantly slowed fibril formation (Figure 3C).

The Iodide−TTR and Chloride−TTR Structures. The crystal structure of the iodide−TTR complex was determined at 1.8 Å and solved with the single-wavelength anomalous dispersion (SAD) method by using the anomalous scattering of the iodide. The anomalous difference Fourier map is shown in Figure 4A. Refinement and automatic interpretation of the electron density map using warpNtrace built 209 of the 230 amino acids included in the final model (Figure 4B). The structure, after final refinement, has an *R*-factor of 20.3% (*R*-free = 23.8%) while maintaining good stereochemistry. Overall, the protein structure is very similar to the 1.5 Å native TTR structure (*19*) with a root-mean-square (rms) deviation of only 0.2 Å (see Table 1). From the anomalous

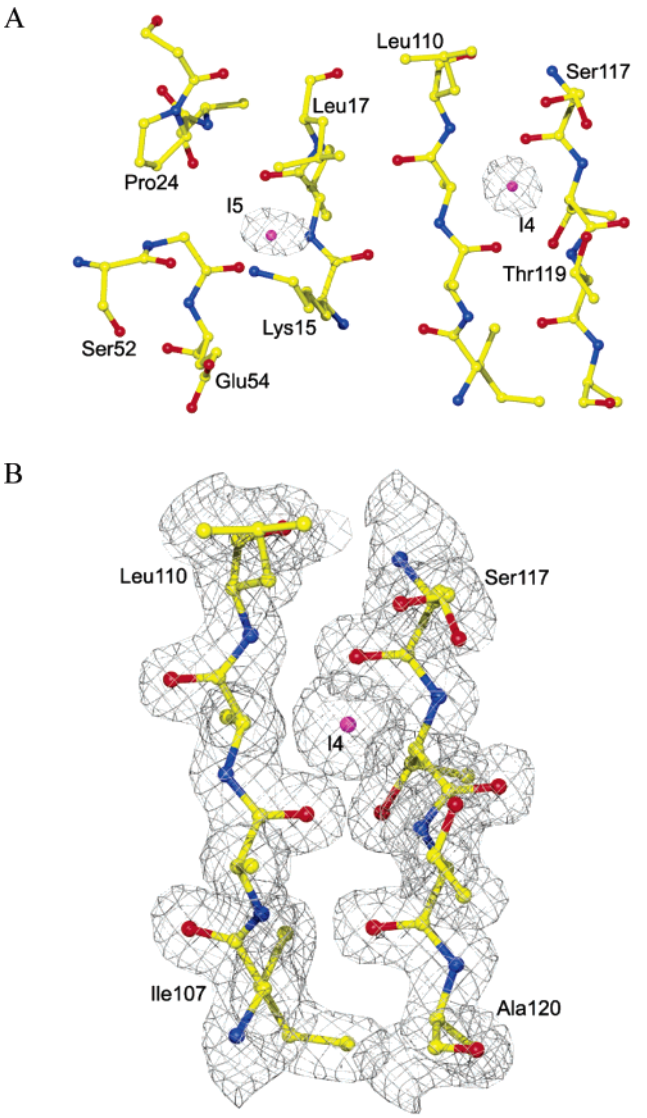

FIGURE 4: Binding site of iodide at the hormone-binding channel of TTR. (A) Depicted are residues from chain B and the anomalous difference Fourier map of the iodide derivate (pink sphere) contoured at 10σ. (B) Shows the quality of the electron-density map produced by warpNtrace. The model is drawn from the refined iodide−TTR structure.

difference map, the binding sites of three iodides were identified at each of the two monomers in the asymmetric unit (named I-1 to I-3 in monomer A and I-4 to I-6 in monomer B). The iodides are well-defined, and five of them have electron densities visible at σ values over 10, where σ is the rms electron density throughout the unit cell. Occupancies for the six iodides were refined and varied between 21 and 91% (see Table 1). The iodide-bound structure comprises residues 10−124 of both monomers of the asymmetric unit. A total of 136 water molecules are positioned within hydrogen-bonding distance (3.3 Å) from the protein or a protein-connected water and with refined temperature factors less than 55 $Å^2$. Out of 36 stabilizing water molecules discussed in Hörnberg et al. (*19*), 28 were included in the structure. Two of the missing water molecules are situated in the hydrophobic core of each monomer (W4 and W7), and their absence is probably due to the lower resolution of the iodide structure compared to the wild-type structure. The positions of four of the remaining missing

solvent molecules (two per monomer) are substituted by the iodides I-1 and I-4. Structural validation was done with the program OOPS2 (*65*). Residues with weak or no density are A-Asp39, A-Lys48, B-Arg103, and B-Arg104. Statistics are presented in Table 1.

The structure of the chloride−TTR complex was determined by Fourier methods at 1.9 Å and refined to a final *R*-factor of 20.0% (*R*-free, 22.1%). Six chlorides (Cl-1 to Cl-6) bound to the TTR dimer at identical sites as the iodides. In an omit map, four chlorides are visible at 5σ, whereas Cl-2 and Cl-5 are visible at 3 and 4σ, respectively. The occupancies for the six chlorides varied between 37 and 57% (Table 1). The same conserved water molecules present in the iodide structure are found in the chloride structure. Residues with weak or no densities are A-Asp39, A-Leu82, A-Ile84, B-Asp39, B-Glu63, B-Pro102, B-Arg103, and B-Arg104.

DISCUSSION

The halogen-binding sites in TTR were first described in the crystal structure of human TTR in complex with thyroxine (T_4) (*29*). The thyroxine molecule contains four iodines, and based on their binding to TTR, the hormone-binding site was divided into an inner and outer cavity comprising three symmetry-related pairs of halogen-binding pockets, HBP1 (HBP1′), HBP2 (HBP2′), and HBP3 (HBP3′) (Figure 5A,B) (*29*). The side chains of Met13, Lys15, and Thr106 define the outer pocket HBP1. The middle pocket HBP2 is composed of the hydrophobic side chains of residues Lys15, Leu17, Ala109, and Leu110, while the main-chain carbonyl groups of Lys15, Ala108, and Ala109 form a hydrophilic surface. The innermost pocket, HBP3, is formed by residues Ala108, Ala109, Leu110, Ser117, Thr118, and Thr119. Like HBP2, it has a hydrophilic surface constituting the main-chain carbonyl oxygens and amino groups of Ala108, Ala109, Leu110, and Thr118 and the polar parts of the Ser117 and Thr119 side chains. In addition to the halogen-binding pockets, Lys15 and Glu54, situated at the entrance of the channel, are involved in hormone binding and interact with the alanyl group of the thyroid hormones. The three halogen-binding pockets were identified from the T_4−TTR complex crystallized in space group $P2_12_12$. In this space group, the asymmetric unit comprises one dimer of the TTR homo-tetramer. The 2-fold symmetry axis of the TTR homo-tetramer, which runs in the direction of the hormone-binding channel, coincides with one of the 2-fold crystallographic axes of this space group. The T_4 ligand, however, lacks 2-fold symmetry, and subsequently, the X-ray structure had to be solved with the ligand positioned in two symmetry-related conformations with 50% occupancy (Figure 5A). This complicated electron density map interpretations and reduced the accuracy of the model. By solving the T_4−TTR complex structure in a new space group with tetramers in the asymmetric unit, aligned T4 molecules in human and rat TTR were obtained (*31*, *66*). However, the contribution of the three individual HBPs for T_4 binding is still not clear.

The precursor molecules for thyroxine synthesis are iodide ions and tyrosyl residues (for a review see ref *67*). We discovered the iodide-binding properties of TTR during crystallization with an additive screen (Hampton Research).

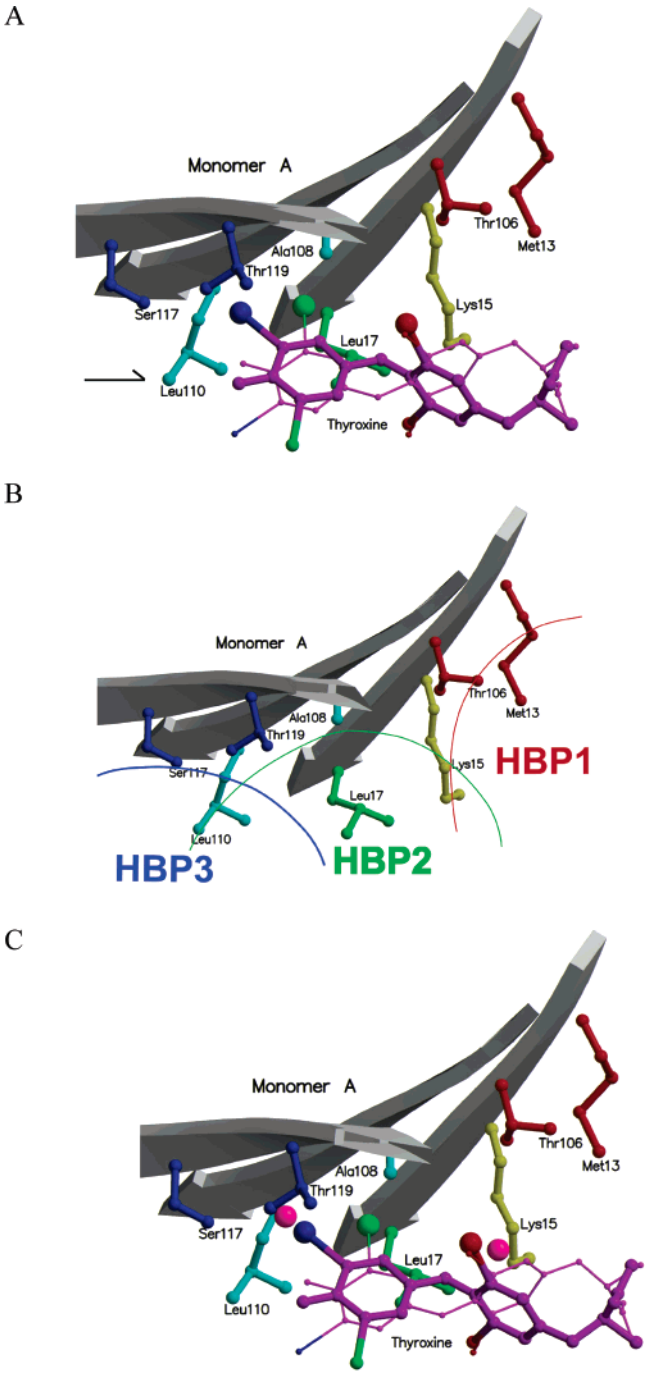

FIGURE 5: The thyroid hormone-binding site in human transthyretin. (A) The thyroxine−TTR complex is drawn from the structure determined by Wojtczak et al., pdb code 2ROX (*29*). The crystallographic 2-fold symmetry-axis, which runs through the center of the homotetramer, is indicated with a black arrow. This axis, combined with the asymmetric binding of the T_4 molecule, positions two symmetry-related conformations of the T_4 molecule on top of each other. The two T_4 conformations are shown as magenta, one thick and the other thin. Residues involved are colored coded as follows: HBP1, red; HBP1 and HBP2, yellow; HBP2, green; HBP2 and HBP3, light blue; HBP3, dark blue. (B) Shows the approximate position of the three halogen-binding sites in the TTR monomer. (C) Binding site of the halide atoms at the dimer−dimer interface. The view is the same as in panel A but including two bound iodides shown as pink spheres.

Large, yellow crystals were obtained in the presence of 0.4 M KI, and the structure was solved by the SAD method at 1.8 Å resolution. During the progress of this work, chloride ions were reported to have stabilizing effects on the tet-

Table 2: Atomic Distances (D < 4.2 Å) between the Transthyretin Molecule and Bound Iodide (I^-), Chloride (Cl^-), and Thyroxine (T_4)[a]

halide(s)	HBP1	D (Å)	halide(s)	HBP2	D (Å)	halide(s)	HBP3	D (Å)
				T_4				
I3	Lys15CE	4.0 (-)	I3′	Leu17′CD2	3.7 (-)	I5′	Ala108O	4.1 (3.7)
	Leu17CD1	3.2 (3.2)		Ala108′CB	3.9 (3.9)		Leu110CB	3.5 (3.8)
	Leu17CD2	4.2 (-)		Ala109′O	2.8 (3.3)		Leu110N	3.5 (3.7)
	Ala108′CB	- (3.9)		Ala109′N	3.5 (3.7)		Ser117O	3.9 (3.8)
	Val121′CG2	- (3.9)		Leu110′CB	4.2 (4.2)		Ser117OG	- (4.1)
				Leu110′N	3.7 (3.9)			
				Leu17CG	3.7 (3.6)			
				I^-				
I-2(5)	Lys15CE	3.5 (3.4)				I-1(4)	Ala108O	4.1 (4.1)
	Lys15NZ	3.8 (3.5)					Leu110CB	4.1 (4.1)
	Leu17CD2	- (4.2)					Leu110N	4.1 (4.1)
	Val121′CG2	4.0 (-)					Ser117O	3.9 (3.8)
	W′134	3.3 (-)					Ser117OG	3.2 (3.6)
	W′105	- (4.2)					Ser117*OG	- (3.4)
							Thr119OG1	3.3 (3.3)
				Cl^-				
Cl-2(5)	Lys15CE	3.7 (3.3)				Cl-1(4)	Ala108O	3.8 (3.7)
	Lys15NZ	3.2 (3.3)					Leu110CB	4.2 (-)
	Leu17CD2	4.0 (4.2)					Leu110N	4.0 (4.2)
	Val121′CG2	3.6 (3.9)					Leu110′CD2	- (4.1)
	Val121′CB	4.1 (-)					Ser117O	3.4 (3.5)
							Ser117OG	2.9 (2.9)
							Thr119OG1	3.0 (2.9)
							W35	3.1 (−)

[a] Symmetry-related molecules are indicated with ′, and alternate conformations are indicated with *.

rameric TTR structure (*50*). This finding induced us to extend our structural study to include a characterization of the chloride-binding sites.

Halides, in contrast to metal ions, bind unspecifically to proteins and show no preferences for specific coordination geometries. By forming hydrogen bonds with hydrogen-bond donor groups of the protein or by binding through hydrophobic interactions, halide ions are able to substitute water sites around the protein surface. In X-ray structures, the highest occupancies for halide ions occur when ion pairs are formed with positively charged Arg or Lys side chains (*68*). Other types of studies have found that iodide ions also interact with main-chain amide groups with some preference for amino acids Trp, Phe, Tyr, Leu, Gly, Arg, and Asn, side-chain nitrogens of Gln and Asn, and the hydroxyl group of Ser (*69*).

In both the iodide− and chloride−TTR structures, three ions were found bound to each TTR monomer. The positions of the iodides were identified from their strong anomalous signal (Figure 4A), whereas the positions of the chlorides were identified from their high sigma values in difference Fourier maps (see Table 1).

Two of the iodide- and chloride-binding sites are situated at previously identified halogen-binding pockets: one at HBP1 (referred to as I-2 or Cl-2 in monomer A, and I-5 or Cl-5 in monomer B) and one at HBP3 (I-1 or Cl-1 in monomer A, and I-4 or Cl-4 in monomer B) (Figure 5C). The ion situated at the innermost HBP3 pocket is bound with the highest occupancy (see Table 1). This pocket is also more polar than HBP1, and the bound anion interacts with both the hydroxyl groups of the side chains of Ser117 and Thr119 and with the main-chain nitrogen and oxygen atoms of Leu110 and Ala108. The anion situated at HBP1 forms an ion pair to the side chain of Lys15 and hydrophobic contacts with Leu17 and Val121′ (where ′ symbolizes a symmetry-related residue, Table 2).

TTR has been structurally characterized in complex with three other iodine-substituted compounds in addition to thyroxine (*29*, *31*). These are diiodo-L-thyronine (*70*), tetraiodo-thyroacetic acid (*71*) ,and iododiflunisal (*72*). Overall, the conformation of TTR in the anion-bound form is very similar to the conformations of the protein in complex. Iododiflunisal binds with its sole iodine-substituted phenyl ring positioned close to the entrance of the hormone-binding channel, and the iodine binds to HBP1 (*72*). The carboxylate substituents of T_4, diiodo-L-thyronine, and iododiflunisal are placed approximately in the same position at the entrance of the hormone-binding channel allowing direct interaction with the Nϵ atom of Lys15. This orientation is generally referred to as the "forward"-binding mode. The side chain of Lys15 is situated in the vicinity of Glu54 in wtTTR, but without direct contacts to neighboring residues; however, its side chain is poorly defined (*19*). This is not the case for the anion-bound and the ligand-bound structures, in which an ion pair formed with Lys15 makes its side chain well-defined in the electron density. Diclofenac, the only inhibitor with a chlorine-substituted phenyl ring that has been structurally characterized, binds in the "reverse" mode. In this position, the negatively charged carboxyl substituent of the ligand is situated at HBP3, which allows direct hydrogen-bond interaction between the carboxyl group and the side chains of Ser117 and Thr 119 (*44*). The chlorines of dichlofenac are situated in the vicinity of HBP1 and HBP1′ (*44*). Tetraiodo-thyroacetic acid binds in both the forward and reverse conformation with equal occupancy (*71*).

The third anion, I-3 or Cl-3, is positioned far from the hydrophobic channel at the surface of the monomer, a region we refer to as the saddle (Figure 6). At this site, the anion provides stability to the TTR dimer, bridging the A and B monomers by interacting with the side chains of Lys35 from one monomer and the side chain of His90 from the other. The side chains of Trp41, Ile68, and Val94 are also situated

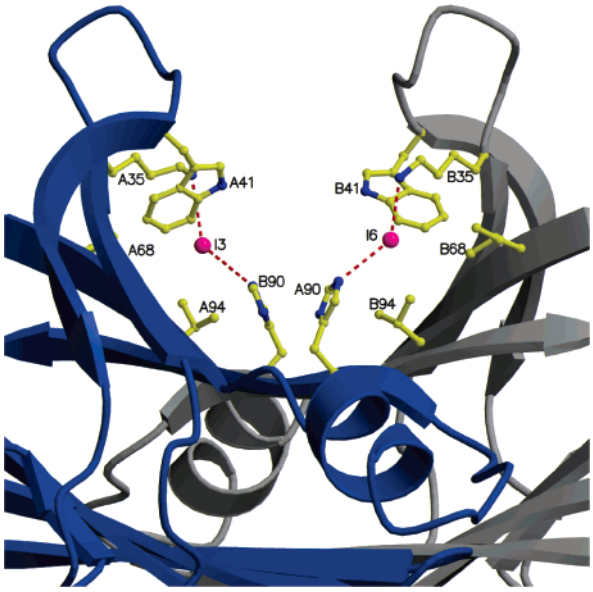

FIGURE 6: Binding site of the halide atoms at the dimer interface (saddle). Depicted are two iodides; however, the chlorides bind essentially at the same site. Each iodide bridges two monomers. Short distances of 3.0−3.6 Å between the halides and the side-chain nitrogen atoms of Lys35 and His90 suggest that the halides bind to this site through ion-pair formation.

in the vicinity of this iodide- and chloride-binding site (<4.5 Å).

We have shown that iodides stabilize the native conformation of TTR both thermodynamically and kinetically to a much larger extent than chlorides. At iodide concentrations in the 0.1−0.2 M range, the wild-type protein was impossible to denature in 6 M urea, for at least 120 h. In the same experiments by Hammarström et al. (*50*) and repeated in this study, 1.5−1.8 M of chloride was needed to reach the same level of stabilization. We propose that precipitation studies at low pH result in two types of aggregates formed in the presence of salt. One type occurs in the pH range 4.0−5.0 and is known to be associated with amyloid formation (*32*, *42*, *44*, *73*). These aggregates are highly salt-sensitive and occur only if chloride and iodide concentrations are kept at relatively low concentrations, 0.25 and 0.1 M, respectively. However, a large increase in turbidity at pH 4.4 occurred only in the presence of 0.1−0.2 M chloride and not if iodide was substituted for chloride. This effect might be explained by the high-occupancy binding of iodide to the protein at these concentrations. The second type of aggregate observed occurs predominantly at pH < 4 and at relatively high-salt concentrations where the increased hydrophobic effect of Cl^- or I^- leads to decreased solubility of the protein (salting-out effects).

Anions interact with proteins in a variety of ways. Anions salt-out nonpolar groups and salt-in the peptide group and thereby stabilize or denature the proteins following the Hofmeister series (*74*). However, the final effect on protein stability is also influenced by specific properties of the anion, such as direct binding to the protein. Hammarström et al. (*50*) showed that 1.8 M SCN^- stabilizes TTR, although to a lesser extent than 1.8 M Cl^-. According to the Hofmeister series, SCN^- is a strong protein denaturant and should provide less stability to TTR than Cl^-. In our urea-unfolding data, I^- provided a significant increase in TTR stability at low concentrations. Like SCN^-, I^- is a strong denaturant of proteins and this effect on TTR was therefore not to be expected. On the basis of the X-ray structures presented in this work, we propose that the stabilizing effect is most likely due to the direct binding of I^- to TTR. The physiological relevance of iodide binding is not clear. The concentration of iodide needed for amyloid fibril suppression in these experiments was much higher than physiological levels. Thyroxine, for example, significantly reduces the level of TTR aggregation at pH 4.4 in the 10 μM range (*42*). At the same time, it may not be valid to compare the results from rapid experiments in vitro with the slow progression of amyloid fibril formation that takes place in patient tissues.

In conclusion, we have shown that Lys15 is part of a halide-binding site at the HBP1 of the hydrophobic channel of TTR, which provides a structural explanation for the stabilization effects which the anion has on the TTR tetramer (*50*). Furthermore, we demonstrated that HBP3 constitutes a halide-binding site. Some of the inhibitors of amyloid formation in TTR are known to bind to the hormone-binding channel in the so-called "reverse" conformation; that is, their negatively charged carboxyl groups bind at HBP3 (*44*, 75). One could therefore imagine that other negatively charged groups properly positioned on the inhibitor might preferentially bind at this site as well and thereby contribute to the overall stabilization of the native TTR structure to prevent the onset of amyloid fibril formation.

ACKNOWLEDGMENT

We thank Dr. Therese Eneqvist for helpful discussions and Terese Bergfors for critical reading of the manuscript.

REFERENCES

1. Cohen, A. S., and Jones, L. A. (1991) Amyloidosis, *Curr. Opin. Rheumatol. 3*, 125−138.
2. Schreiber, G., and Richardson, S. J. (1997) The evolution of gene expression, structure and function of transthyretin, *Comp. Biochem. Physiol., Part B: Biochem. Mol. Biol. 116*, 137−160.
3. Hamilton, J. A., and Benson, M. D. (2001) Transthyretin: a review from a structural perspective, *Cell Mol. Life Sci. 58*, 1491−521.
4. Liz, M. A., Faro, C. J., Saraiva, M. J., and Sousa, M. M. (2004) Transthyretin, a new cryptic protease, *J. Biol. Chem. 279*, 21431−21438.
5. Nilsson, S. F., Rask, L., and Peterson, P. A. (1975) Studies on thyroid hormone-binding proteins. II. Binding of thyroid hormones, retinol-binding protein, and fluorescent probes to prealbumin and effects of thyroxine on prealbumin subunit self-association, *J. Biol. Chem. 250*, 8554−8563.
6. Schreiber, G., Southwell, B. R., and Richardson, S. J. (1995) Hormone delivery systems to the brain-transthyretin, *Exp. Clin. Endocrinol. Diabetes 103*, 75−80.
7. Hagen, G. A., and Elliott, W. J. (1973) Transport of thyroid hormones in serum and cerebrospinal fluid, *J. Clin. Endocrinol. Metab. 37*, 415−422.
8. Herbert, J., Wilcox, J. N., Pham, K. T., Fremeau, R. T., Jr., Zeviani, M., Dwork, A., Soprano, D. R., Makover, A., Goodman, D. S., Zimmerman, E. A., et al. (1986) Transthyretin: a choroid plexus-specific transport protein in human brain. The 1986 S. Weir Mitchell award, *Neurology 36*, 900−911.
9. Benson, M. D., and Uemichi, T. (1996) Transthyretin amyloidosis, *Amyloid 3*, 44−56.
10. Saraiva, M. J. (1995) Transthyretin mutations in health and disease, *Hum. Mutat. 5*, 191−196.
11. Connors, L. H., Richardson, A. M., Théberge, R., and Costello, C. E. (2000) Tabulation of transthyretin (TTR) variants as of 1/1/2000, *Amyloid 7*, 54−69.
12. Eneqvist, T., and Sauer-Eriksson, A. E. (2001) Structural distribution of mutations associated with familial amyloidotic polyneuropathy in human transthyretin, *Amyloid 8*, 149−168.

13. Saraiva, M. J. (2001) Transthyretin mutations in hyperthyroxinemia and amyloid diseases, *Hum. Mutat. 17*, 493−503.
14. Westermark, P., Sletten, K., Johansson, B., and Cornwell, G. G. D. (1990) Fibril in senile systemic amyloidosis is derived from normal transthyretin, *Proc. Natl. Acad. Sci. U.S.A. 87*, 2843−2845.
15. Sousa, M. M., Cardoso, I., Fernandes, R., Guimaraes, A., and Saraiva, M. J. (2001) Deposition of transthyretin in early stages of familial amyloidotic polyneuropathy: evidence for toxicity of nonfibrillar aggregates, *Am. J. Pathol. 159*, 1993−2000.
16. Andersson, K., Olofsson, A., Nielsen, E. H., Svehag, S. E., and Lundgren, E. (2002) Only amyloidogenic intermediates of transthyretin induce apoptosis, *Biochem. Biophys. Res. Commun. 294*, 309−314.
17. Blake, C. C., Geisow, M. J., Oatley, S. J., Rérat, B., and Rérat, C. (1978) Structure of prealbumin: secondary, tertiary and quaternary interactions determined by Fourier refinement at 1.8 Å, *J. Mol. Biol. 121*, 339−356.
18. Hamilton, J. A., Steinrauf, L. K., Braden, B. C., Liepnieks, J., Benson, M. D., Holmgren, G., Sandgren, O., and Steen, L. (1993) The X-ray crystal structure refinements of normal human transthyretin and the amyloidogenic Val-30 → Met variant to 1.7-Å resolution, *J. Biol. Chem. 268*, 2416−2424.
19. Hörnberg, A., Eneqvist, T., Olofsson, A., Lundgren, E., and Sauer-Eriksson, A. E. (2000) A comparative analysis of 23 structures of the amyloidogenic protein transthyretin, *J. Mol. Biol. 302*, 649−669.
20. Terry, C. J., Damas, A. M., Oliveira, P., Saraiva, M. J., Alves, I. L., Costa, P. P., Matias, P. M., Sakaki, Y., and Blake, C. C. (1993) Structure of Met30 variant of transthyretin and its amyloidogenic implications, *EMBO J. 12*, 735−741.
21. Hamilton, J. A., Steinrauf, L. K., Braden, B. C., Murrell, J. R., and Benson, M. D. (1996) Structural changes in transthyretin produced by the Ile 84 Ser mutation which result in decreased affinity for retinol-binding protein, *Amyloid 3*, 1−12.
22. Schormann, N., Murrell, J. R., and Benson, M. D. (1998) Tertiary structures of amyloidogenic and non-amyloidogenic transthyretin variants: new model for amyloid fibril formation, *Amyloid 5*, 175−187.
23. Damas, A. M., Ribeiro, S., Lamzin, V. S., Palha, J. A., and Saraiva, M. J. (1996) Structure of the Val122Ile variant transthyretin—a cardiomyopathic mutant, *Acta Crystallogr. D52*, 966−972.
24. Sebastião, M. P., Saraiva, M. J., and Damas, A. M. (1998) The crystal structure of amyloidogenic Leu55 → Pro transthyretin variant reveals a possible pathway for transthyretin polymerization into amyloid fibrils, *J. Biol. Chem. 273*, 24715−24722.
25. Eneqvist, T., Olofsson, A., Ando, Y., Miyakawa, T., Katsuragi, S., Jass, J., Lundgren, E., and Sauer-Eriksson, A. E. (2002) Disulfide-bond formation in the transthyretin mutant Y114C prevents amyloid fibril formation in vivo and in vitro, *Biochemistry 41*, 13143−13151.
26. Monaco, H. L., Mancia, F., Rizzi, M., and Coda, A. (1994) Crystallization of the macromolecular complex transthyretin-retinol-binding protein, *J. Mol. Biol. 244*, 110−113.
27. Monaco, H. L., Rizzi, M., and Coda, A. (1995) Structure of a complex of two plasma proteins: transthyretin and retinol-binding protein, *Science 268*, 1039−1041.
28. Naylor, H. M., and Newcomer, M. E. (1999) The structure of human retinol-binding protein (RBP) with its carrier protein transthyretin reveals an interaction with the carboxy terminus of RBP, *Biochemistry 38*, 2647−2653.
29. Wojtczak, A., Cody, V., Luft, J. R., and Pangborn, W. (1996) Structures of human transthyretin complexed with thyroxine at 2.0Å resolution and 3′,5′-dinitro-*N*-acetyl-L-thyronine at 2.2Å resolution, *Acta Crystallogr. D52*, 758−765.
30. Steinrauf, L. K., Hamilton, J. A., Braden, B. C., Murrell, J. R., and Benson, M. D. (1993) X-ray crystal structure of the Ala-109 → Thr variant of human transthyretin which produces euthyroid hyperthyroxinemia, *J. Biol. Chem. 268*, 2425−2430.
31. Wojtczak, A., Neumann, P., and Cody, V. (2001) Structure of a new polymorphic monoclinic form of human transthyretin at 3 Å resolution reveals a mixed complex between unliganded and T4-bound tetramers of TTR, *Acta Crystallogr. D57*, 957−967.
32. Lai, Z., Colón, W., and Kelly, J. W. (1996) The acid-mediated denaturation pathway of transthyretin yields a conformational intermediate that can self-assemble into amyloid, *Biochemistry 35*, 6470−6482.
33. Lashuel, H. A., Lai, Z., and Kelly, J. W. (1998) Characterization of the transthyretin acid denaturation pathways by analytical ultracentrifugation: implications for wild-type, V30M, and L55P amyloid fibril formation, *Biochemistry 37*, 17851−17864.
34. Liu, K., Cho, H. S., Lashuel, H. A., Kelly, J. W., and Wemmer, D. E. (2000) A glimpse of a possible amyloidogenic intermediate of transthyretin, *Nat. Struct. Biol. 7*, 754−757.
35. Jiang, X., Smith, C. S., Petrassi, H. M., Hammarstrom, P., White, J. T., Sacchettini, J. C., and Kelly, J. W. (2001) An engineered transthyretin monomer that is nonamyloidogenic, unless it is partially denatured, *Biochemistry 40*, 11442−11452.
36. Ferrao-Gonzales, A. D., Souto, S. O., Silva, J. L., and Foguel, D. (2000) The preaggregated state of an amyloidogenic protein: hydrostatic pressure converts native transthyretin into the amyloidogenic state, *Proc. Natl. Acad. Sci. U.S.A. 97*, 6445−6450.
37. Eneqvist, T., Andersson, K., Olofsson, A., Lundgren, E., and Sauer-Eriksson, A. E. (2000) The β-slip: a novel concept in transthyretin amyloidosis, *Mol. Cell 6*, 1207−1218.
38. Olofsson, A., Ippel, H. J., Baranov, V., Horstedt, P., Wijmenga, S., and Lundgren, E. (2001) Capture of a dimeric intermediate during transthyretin amyloid formation, *J. Biol. Chem. 276*, 39592−39599.
39. Olofsson, A., Ippel, J. H., Wijmenga, S. S., Lundgren, E., and Ohman, A. (2003) Probing solvent accessibility of transthyretin-amyloid by solution NMR spectroscopy, *J. Biol. Chem*.
40. Serag, A. A., Altenbach, C., Gingery, M., Hubbell, W. L., and Yeates, T. O. (2001) Identification of a subunit interface in transthyretin amyloid fibrils: evidence for self-assembly from oligomeric building blocks, *Biochemistry 40*, 9089−9096.
41. Serag, A. A., Altenbach, C., Gingery, M., Hubbell, W. L., and Yeates, T. O. (2002) Arrangement of subunits and ordering of beta-strands in an amyloid sheet, *Nat. Struct. Biol. 9*, 734−739.
42. Miroy, G. J., Lai, Z., Lashuel, H. A., Peterson, S. A., Strang, C., and Kelly, J. W. (1996) Inhibiting transthyretin amyloid fibril formation via protein stabilization, *Proc. Natl. Acad. Sci. U.S.A. 93*, 15051−15056.
43. Peterson, S. A., Klabunde, T., Lashuel, H. A., Purkey, H., Sacchettini, J. C., and Kelly, J. W. (1998) Inhibiting transthyretin conformational changes that lead to amyloid fibril formation, *Proc. Natl. Acad. Sci. U.S.A. 95*, 12956−12960.
44. Klabunde, T., Petrassi, H. M., Oza, V. B., Raman, P., Kelly, J. W., and Sacchettini, J. C. (2000) Rational design of potent human transthyretin amyloid disease inhibitors, *Nat. Struct. Biol. 7*, 312−321 (published erratum appears in (2000) *Nat. Struct. Biol. 7*, 431).
45. Hammarström, P., Wiseman, R. L., Powers, E. T., and Kelly, J. W. (2003) Prevention of transthyretin amyloid disease by changing protein misfolding energetics, *Science 299*, 713−716.
46. Adamski-Werner, S. L., Palaninathan, S. K., Sacchettini, J. C., and Kelly, J. W. (2004) Diflunisal analogues stabilize the native state of transthyretin. Potent inhibition of amyloidogenesis, *J. Med. Chem. 47*, 355−374.
47. Razavi, H., Palaninathan, S. K., Powers, E. T., Wiseman, R. L., Purkey, H. E., Mohamedmohaideen, N. N., Deechongkit, S., Chiang, K. P., Dendle, M. T., Sacchettini, J. C., and Kelly, J. W. (2003) Benzoxazoles as transthyretin amyloid fibril inhibitors: synthesis, evaluation, and mechanism of action, *Angew. Chem., Int. Ed. 42*, 2758−2761.
48. Green, N. S., Palaninathan, S. K., Sacchettini, J. C., and Kelly, J. W. (2003) Synthesis and characterization of potent bivalent amyloidosis inhibitors that bind prior to transthyretin tetramerization, *J. Am. Chem. Soc. 125*, 13404−13414.
49. Sekijima, Y., Hammarstrom, P., Matsumura, M., Shimizu, Y., Iwata, M., Tokuda, T., Ikeda, S., and Kelly, J. W. (2003) Energetic characteristics of the new transthyretin variant A25T may explain its atypical central nervous system pathology, *Lab. Invest. 83*, 409−417.
50. Hammarström, P., Jiang, X., Deechongkit, S., and Kelly, J. W. (2001) Anion shielding of electrostatic repulsions in transthyretin modulates stability and amyloidosis: insight into the chaotrope unfolding dichotomy, *Biochemistry 40*, 11453−11459.
51. McPherson, A. (1982) *Preparation and Analysis of Protein Crystals*, John Wiley and Sons, New York.
52. Sauer, U. H., and Ceska, T. A. (1997) A simple method for making reproducible fibre loops for protein cryocrystallography, *J. Appl. Crystallog. 30*, 71−72.
53. Otwinowski, Z., and Minor, W. (1997) Processing of X-ray diffraction data collected in oscillation mode, *Methods Enzymol. 276*, 307−326.
54. Brünger, A. T., Adams, P. D., Clore, G. M., DeLano, W. L., Gros, P., Grosse-Kunstleve, R. W., Jiang, J. S., Kuszewski, J., Nilges, M., Pannu, N. S., Read, R. J., Rice, L. M., Simonson, T., and

Warren, G. L. (1998) Crystallography & NMR system: a new software suite for macromolecular structure determination, *Acta Crystallogr. D54*, 905−921.
55. Brünger, A. T. (1992) Free R value: a novel statistical quantity for assessing the accuracy of crystal structures, *Nature 355*, 472−474.
56. Perrakis, A., Morris, R., and Lamzin, V. S. (1999) Automated protein model building combined with iterative structure refinement, *Nat. Struct. Biol. 6*, 458−463.
57. Morris, R. J., Perrakis, A., and Lamzin, V. S. (2003) ARP/wARP and automatic interpretation of protein electron density maps, *Methods Enzymol. 374*, 229−244.
58. Jones, T. A., Zou, J. Y., Cowan, S. W., and Kjeldgaard. (1991) Improved methods for binding protein models in electron density maps and the location of errors in these models, *Acta Crystallogr. A47*, 110−119.
59. Collaborative Computational Project, N. (1994) The CCP4 suite: programs for protein crystallography, *Acta Crystallogr. D50*, 760−763.
60. Murshudov, G. N., Vagin, A. A., and Dodson, E. J. (1997) Refinement of macromolecular structures by the maximum-likelihood method, *Acta Crystallogr. D53*, 240−255.
61. Schomaker, V., and Trueblood, K. N. (1968) On the rigid-body motion of molecules in crystals, *Acta Crystallogr. B24*, 63−76.
62. Winn, M. D., Isupov, M. N., and Murshudov, G. N. (2001) Use of TLS parameters to model anisotropic displacements in macromolecular refinement, *Acta Crystallogr. .D57*, 122−133.
63. Colon, W., and Kelly, J. W. (1992) Partial denaturation of transthyretin is sufficient for amyloid fibril formation in vitro, *Biochemistry 31*, 8654−8660.
64. Pettersson, T., Carlstrom, A., and Jornvall, H. (1987) Different types of microheterogeneity of human thyroxine-binding prealbumin, *Biochemistry 26*, 4572−4583.
65. Kleywegt, G. J. (2000) Validation of protein crystal structures, *Acta Crystallogr. D56* (Pt 3), 249−265.
66. Wojtczak, A., Cody, V., Luft, J. R., and Pangborn, W. (2001) Structure of rat transthyretin (rTTR) complex with thyroxine at 2.5 Å resolution: first non-biased insight into thyroxine binding reveals different hormone orientation in two binding sites, *Acta Crystallogr. D57*, 1061−1070.
67. Shen, D. H., Kloos, R. T., Mazzaferri, E. L., and Jhian, S. M. (2001) Sodium iodide symporter in health and disease, *Thyroid 11*, 415−425.
68. Dauter, Z., Dauter, M., and Rajashankar, K. R. (2000) Novel approach to phasing proteins: derivatization by short cryo-soaking with halides, *Acta Crystallogr. D56* (Pt 2), 232−237.
69. Evans, G., and Bricogne, G. (2002) Triiodide derivatization and combinatorial counter-ion replacement: two methods for enhancing phasing signal using laboratory Cu Kalpha X-ray equipment, *Acta Crystallogr. D58*, 976−991.
70. Wojtczak, A., Luft, J., and Cody, V. (1992) Mechanism of molecular recognition. Structural aspects of 3,3′-diiodo-L-thyronine binding to human serum transthyretin, *J. Biol. Chem. 267*, 353−357.
71. Muziol, T., Cody, V., Luft, J. R., Pangborn, W., and Wojtczak, A. (2001) Complex of rat transthyretin with tetraiodothyroacetic acid refined at 2.1 and 1.8 Å resolution, *Acta Biochim. Pol. 48*, 877−884.
72. Gales, L., Macedo-Ribeiro, S., Arsequell, G., Valencia, G., Saraiva, M. J., and Damas, A. M. (2005) Human transthyretin in complex with iododiflunisal—structural features associated with a potent amyloid inhibitor, *Biochem. J. 388*, 615−621.
73. Lashuel, H. A., Wurth, C., Woo, L., and Kelly, J. W. (1999) The most pathogenic transthyretin variant, L55P, forms amyloid fibrils under acidic conditions and protofilaments under physiological conditions, *Biochemistry 38*, 13560−13573.
74. Baldwin, R. L. (1996) How Hofmeister ion interactions affect protein stability, *Biophys. J. 71*, 2056−2063.
75. Ghosh, M., Meerts, I. A., Cook, A., Bergman, A., Brouwer, A., and Johnson, L. N. (2000) Structure of human transthyretin complexed with bromophenols: a new mode of binding [in process citation], *Acta Crystallogr. D56*, 1085−1095.

BI050249Z